University of Washington

ME 495

Mechatronics Capstone Design Report

Series Elastic Actuator Report

Authors
Nikolas Johnson
Zachary Taylor
James Muir
Talal Abdullah
Xinyu Hou

Supervisor
Dr. Joseph Garbini

June 13, 2020

Contents

List of Figures

List of Tables

1 Executive Summary

The desire to increase productivity in industrial manufacturing and assistive service applications presents our world with the challenge of creating a safe environment for human robot interaction. Traditional actuators are designed to be stiff to achieve a high bandwidth, which is ideal for a precise position control and shortens the system's response time to a change in the input. However, it raises safety concerns which limits the range of available human-robot interaction due to unstable force control and low shock tolerance[7]. Series Elastic Actuators (SEAs) address this issue by including an elastic element in the force transmission. They trade off high bandwidth for more stable force control, high fidelity, high backdrivability, high shock tolerance and output impedance and thus provide safer physical interactions between humans and robots [11].

Due to the wide range and diversity of SEA applications, this project focuses on designing and implementing a proof of concept prototype of a tabletop MARIONET (Moment arm Adjustment for Remote Induction of Net Effective Torque) style SEA, a simple version of an SEA that utilizes cable-driven transmission with two equal-sized pulleys and two elastic elements connected in parallel [8]. The design is divided into several sections: basic description, assumptions, mechanical, control, electrical, embedded software, and system integration. The construction of the prototype is described and comparisons between experimental performance and design analysis is provided.

We also included an analysis of risk and liability, ethical issues, impacts on the society and the environment, cost and engineering economics, and consistency with the engineering codes and standards, all with respect to our SEA design. Future development of the project including improvements in both the mechanical and controller design, and the final product configurations are given in the conclusion.

Two different block diagrams and their corresponding transfer functions were designed, modeled using MATLAB and implemented to control the prototype. The construction of the prototype was a success. We faced a few setbacks during assembly, but eventually succeeded in creating a mechanically functioning prototype. Testing results show that the single-loop block diagram model did not perform as intended in the position tracking test, as the voltage output of the controller was too low to drive the motor. On the other hand, the double loop controller model performed very well in the position and torque reference tracking tests. The torque reference tracking test was performed by fixing the output position and providing a reference torque profile. The position reference tracking test was performed by fixing a 0.509 kg mass to the load and providing a reference position profile, while the position disturbance rejection test used the same mechanical setup but set the reference position to zero and measured the ability of the system to return to that fixed setpoint after an position disturbance.

2 Introduction

2.1 Problem Definition

With a typical stiff actuator, human-robot interactions can be dangerous, in part because small disturbances can result in large output forces. Other issues with stiff actuators include excessive noise and contact instability. All these lead to potential safety hazards in non-structured working environments. One solution to this problem is to add compliance/elastic elements to the actuator. Adding compliance/elasticity to the actuator allows for small disturbances to be absorbed without resulting in large force outputs, which helps address safety concerns. However, the elastic element makes controlling the actuator more difficult, a problem that we address later in the report.

The primary objectives of our SEA design are to achieve safer human-robot interaction while maintaining effective position and force control. Our first

step was performing a preliminary research on SEAs. We looked at commercial products currently on the market and at papers that focused on the design and control of SEAs. Based on our project requirements and our research into existing SEA designs, we have decided that our prototype will be roughly tabletop sized: small enough to comfortably be worked with on a lab bench but large enough to not complicate prototype production. We decided to pursue a MARIONET [8] style design which utilizes cables to transmit tension between two equally sized pulleys, for its larger range of motion in a relatively compact size.

2.2 Functional Requirements

We identified important functional specifications for an SEA and compiled sample values for each from various sources including research papers and commercial product specifications such as the Hebi X and R Series SEA [14]. Important functional specifications include the actuator's maximum continuous torque output, the percent overshoot and settling time of the transient response, and the frequency response bandwidth. We averaged the collected values for each functional specification to produce our target specifications in an effort to achieve a design for a mid-ranged capability SEA, with the exception that our output torque would need to be lower to ensure the feasibility of our prototype fabrication. Our targeted functional specifications are listed in Table 1.

Table 1: Functional specifications of SEA design

Functional Specification	Value
Max Torque Output (continuous)(Nm)	0.5
Overshoot (%)	16
Settling Time (s)	0.19
Bandwidth (Hz)	21.5

2.3 Case Study

In our early research stage, we closely investigated two successful industry-level SEA implementations that inspired our final prototype design.

The first focused on a small-scale exoskeleton SEA for hand rehabilitation, produced by researchers at the University of Texas at Austin [2]. The small-scale solution provided by Deshpande A. et al., proposed an alternative for traditional exoskeleton actuators that have high reflected inertia and non-linearity in friction. Their design focused on reducing the model size by using a remotely located actuator and Bowden cables for force transmission. As opposed to our final controller design, the controllers of Deshpande A. et al. used an inner position control loop and an outer force control loop with the ultimate goal of accurate force control. Their device utilized load cells and encoders for force and position feedback.

The second design was implemented by Isik K. et al, named the StoneAge SEA [4]. The StoneAge design served as a reference for some of the primary design assumptions our team utilized for our model. One such idea was to assume a very low load impedance when designing our force control loop. This assumption simplifies the system model by assuming that the output position is fixed, equivalent to an infinitely large load inertia. This is achieved by grounding the SEA output in the controller design as shown in the simplified linear graph (Fig. 9) below [4]. This assumption is justified when the force control loop operates faster than the load position can respond. The Stone-Age control system block diagram with a force control loop and angle control loop inspired the implementation of our torque and position control loops.

3 The Design

3.1 Description

In our investigation of multiple successful applications of SEA technology, three main design criteria were the most influential in our path to a preliminary design. Those three aspects were: 1. the scale of the design: a medium-sized model approximately one cubic foot large was desired for its manufacturability and the prevalence of motors available at that scale; 2. position and torque control through two encoders; and 3. the ease of manufacturing the prototype.

Our design is modeled after a MARIONET style SEA [8]. It features an input pulley driven by a motor and an output pulley that the load is attached to. A rough sketch is pictured in Figure 1. The pulleys are linked by a belt (fishing line in our case) that has elastic elements (springs). These springs can deform allowing a deviation between the angular positions of the pulleys. The springs are in series with the motor and the load, thus our design meets the basic requirements to be a Series Elastic Actuator.

3.2 Assumptions

The following assumptions are made for the design of this SEA:

- The output position is fixed when deriving the torque control loop.
- The inner torque control loop operates approximately 10 times faster than the outer position control loop.
- Damping effects due to the motor and the load are negligible.
- Gravitational force is negligible.
- The output torque can be determined by the relative angular positions of the pulleys.

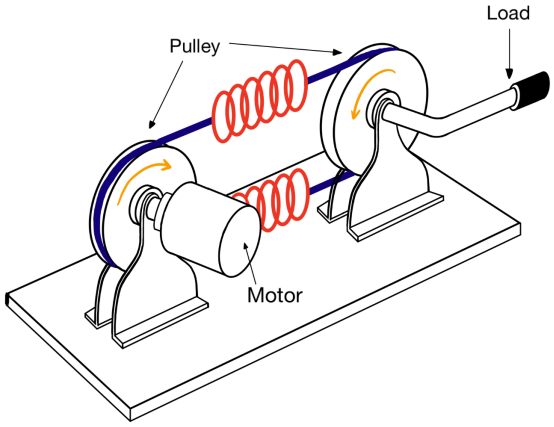

Figure 1: Motor geometry with model assumptions

- A potential feed-forward term for the purpose of improving control accuracy and stability will be ignored for now.

These assumptions were mindfully chosen to allow for a simple preliminary design with a manageable performance and complexity that can be enhanced upon the success of the first prototype.

3.3 Mechanical

The mechanical design of our SEA device was based on the sketch in Figure 1. A CAD model of the final design can be seen in Figure 2. Crucial elements of design included the interfaces and interactions of the pulleys, springs, and cables, the geometry of the load arm to accommodate the desired masses, and the frame/mounting system for the device.

3.3.1 Spring and Cable Choices

Design of the spring and cable components took a force-based approach. The analysis began with two key functional specifications: the maximum motor torque, derived from the HEBI actuators and available parts, and a broad "table top" size goal. From our general scale aspirations a pulley diameter was chosen. Using pulley size and maximum output torque, we were then able to specify spring constants and cable load requirements.

The springs were the first to be defined. As springs with lower spring constants tend to have a lower maximum load tolerance, a balance needed to be stuck between compliance and strength which would satisfy the needs of our design. In addition, most springs have a minimum load limit, where below the limit the springs lose dynamic continuity. This characteristic was also taken into account. Based on these parameters we determine a criteria to pick a number of possible springs. The criteria is derived below in equations 1 to 5, where $F_{applied}$ is known and compared to $F_{max,spring}$ and $F_{min,spring}$, provided by the manufacturer.

$$F_{pre-load} = F_{min,spring} + \frac{1}{2}F_{applied} \tag{1}$$

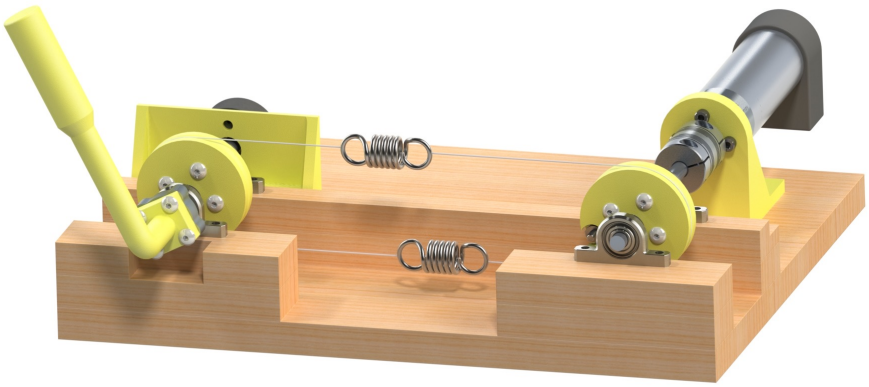

Figure 2: CAD model of the final prototype

$$F_{max,spring} = F_{pre-load} + F_{applied} \tag{2}$$

$$F_{max,spring} = F_{min,spring} + \frac{3}{2}F_{applied} \tag{3}$$

Applied force is half of that produced by the load arm due to motor torque

$$F_{applied} = \frac{T_{stall,motor}}{d_{pulley}} \tag{4}$$

Thus the failure criteria of the springs is as follows:

$$\frac{3}{2}F_{applied} < (F_{max,spring} - F_{min,spring}) \tag{5}$$

With this criteria it was calculated that $F_{max,spring} - F_{min,spring}$ needed to be 18.75 N (4.22 lbf). A selection of springs was chosen that fit this criteria. The end goal of this project is to design an actuator which will protect a human user through actuator compliance in the case that the actuator is applying a load directly to the human. As such, the stiffness of the spring must be low enough that reasonable deflection is achieved before the entire stall torque of the motor was applied to the person. Thus, the next criteria applied to our spring selection was the max load arm deflection when a stall torque is applied to a person, who is modeled as an immovable object. Equation 6 was used to find this rotational deflection for a number of selected springs, and those with a sufficiently high deflection were chosen for the final prototype. Equation 6 is derived from conversion of the linear spring constant to one which is rotational.

$$\theta_{deflection} = \frac{T_{max}}{r_{pulley}^2 K} \tag{6}$$

The cable was originally intended to be a metal wire rope, however with the decision to go with a smaller pulley size there were concerns over flexibility of the rope and its ability to properly wrap around the small pulleys. Also taking into account the now lower overall load on the spring/cable system, it was decided that fishing line would make a better cable material for its flexibility and strength. Fishing line was analyzed based on the predicted maximum applied load it would need to withstand, using equation 3, with a resulting predicted load of 40.6 N (9.13 lbf) for our system. Another important consideration was the degradation of the cable

strength at the mounting interfaces to the springs and pulleys. The mounting to the springs was of primary concern, as we would need to tie the cable to the springs using a traditional knot. Information was gathered from a popular fishing website [10] which offered rough estimation of knot strength degradation due to knots of at most 62% strength. Looking at available options it was decided that a fishing line rated at 222 N (50 lbf) would offer a sufficient factor of safety of 1.6, and at reasonable cost.

Another concern when choosing our cable was how its compliance would effect our dynamic models. This was particularly important with the decision to switch to fishing line, as it has much more appreciable compliance than the metal wire rope. The chosen cable was made from a solid nylon cord "monofilament", chosen intentionally for the mechanical predictability of its uniform cross section. The spring constant of the material was determined from Hooke's law with equation 7, where A is the cross sectional area of the monofilament, E is the modulus of elasticity of Nylon, and l is the length of the cable segments. For the selected cable it was determined that the spring constant for each quarter segment was 29.4 kN/m (167.9 lbf/in), or roughly 2.0% of our final chosen spring constant value of 577.9 N/m (3.3 lbf/in). Due to this low contribution, compliance of the cable was considered negligible.

$$K = \frac{AE}{l} \tag{7}$$

The shaft components were based around the 6 mm output shaft of the motor. Two bearing were used on either side of the pulley to provide support in the directions perpendicular to the shaft. Collars were used to keep the shaft in place, and hubs were used to connect the pulleys and load arm to the base of the shaft. Finally couplers were used to connect the motor/gearbox output to the shaft to protect the system from damage due to rotational impulses. Figures 3 and 4 show these shaft components in their final orientations.

The load arm was designed with testing in mind, such that weights of varying mass could be attached to the end to simulate applied loads and inertias. Originally it was intended that a person would simply pull on the output arm to apply the torque as shown in Figure 2, however it was decided that the bare arm had too little inertia for good controller design, and that the applied torques would have limited accuracy. It was determined that a series of sockets of varying sizes would be used as the applied weights, and so a new arm was designed to hold these sockets in place using a circular end stop, an image of which is provided in Figure 5.

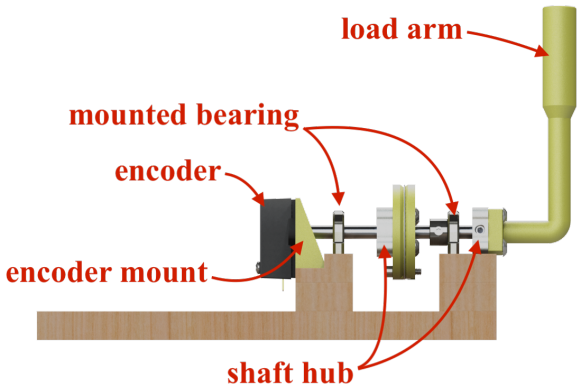

Figure 3: Load side shaft component diagram

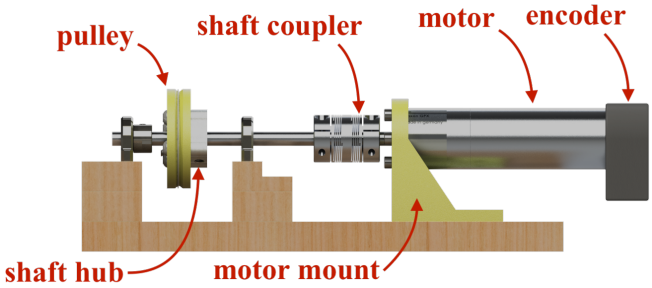

Figure 4: Motor side shaft component diagram

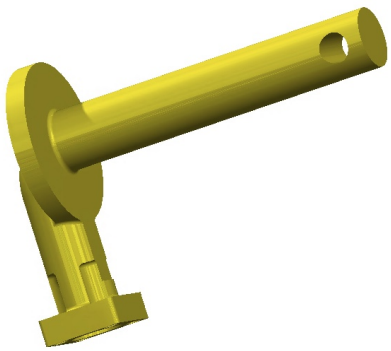

Figure 5: CAD model of the new load arm design, with a backstop for the applied masses

Position of the masses on the arm was carefully chosen in order to achieve an inertia which would result in the desired resonant frequency of the plant. Mechanical analysis was also performed with the given mass loads to ensure structural integrity of the arm. Namely, bending moment equations provided in 8 and torsional shear force provided in 9 were used at the arm straight away and arm bend.

$$\sigma = \frac{Mr}{I} \tag{8}$$

$$\tau = \frac{Tc}{J} \tag{9}$$

The pulley was designed to provide an ample platform for cables and springs to provide the needed compliance, while also being able to efficiently transmit power from the motor. Originally it was intended that the pulleys would be designed as a typical power transmission pulley, where the cables were tensioned such that only friction between them and the pulleys prevented slippage and allowed torque to be transmitted. However, due to the fact that the cables needed to be tied in place to the springs, and the small scale of our project, we were unable to use a typical sized and shaped pulley covered in available mechanical analysis methods. Without a solid way to predict the behavior of the cables on the pulleys, and out of fear of lack of friction leading to slipping, it was decided that the cables would be simply pinned to the pulleys instead. This would cause an increase in complexity of the design, but would ensure proper pulley behavior. Pinning was done using a bolt and nut combination on each pulley.

3.3.2 Mechanical System Parameters

In order to design the controllers and simulate the system we needed to know the system parameters. The important parameters can be found in our overall linear graph (Figure 6).

Early in the design process a simplified model of our prototype was used to analytically derive inertia values for the shaft components. In our final version the inertia values were gathered from our CAD models and from specification sheets provided by part manufacturers. One exception to this is the applied mass at the load arm, which was added separately by assuming it to be the inertia of a point mass of 820 grams, defined by equation 10.

$$I_{Load} = m_{load} r_{load}^2 \tag{10}$$

The spring stiffness value was picked to be $578\,\mathrm{kN\,m^{-1}}$ (3.3 lbf/in), as it fit our criteria defined in section 3.3.1. Using this value for the linear spring constant, a rotational K value was determined using equation 12. All parameters used in simulation are presented in Table 2.

Table 2: Mechanical Parameters of SEA Device

Parameter	Unit	Value
J_m	$\mathrm{kg\,m^2}$	2.14×10^{-6}
J_g	$\mathrm{kg\,m^2}$	1.31×10^{-7}
J_{p1}	$\mathrm{kg\,m^2}$	2.871×10^{-6}
J_{p2}	$\mathrm{kg\,m^2}$	2.871×10^{-6}
J_L	$\mathrm{kg\,m^2}$	1.981×10^{-3}
R_1	m	2×10^{-2}
R_2	m	2×10^{-2}
R_g	unitless ratio	1:16
K_1	$\mathrm{N\,m^{-1}}$	578
K_2	$\mathrm{N\,m^{-1}}$	578
K_{vi}	$\mathrm{A\,V^{-1}}$	0.41
K_t	$\mathrm{N\,m\,A^{-1}}$	0.0214
$J_{p1,extra}$	$\mathrm{kg\,m^2}$	3.528×10^{-6}
$J_{p2,extra}$	$\mathrm{kg\,m^2}$	1.398×10^{-6}

3.4 Control

To control our SEA device, we used feedback controllers. We tried two controller architectures. The first one consisted of a single position control loop (Figure 7) which we called the single loop design. The second one consisted of an outer position control loop with an inner torque control loop (Figure 8). We called the second one the double loop design.

3.4.1 Single Loop Controller

$$K = K_1 + K_2$$
$$J_1 = J_m + J_g$$
$$J_2 = J_{p2} + J_L$$

$$\frac{\Theta_L}{\Theta_{ref}} = \frac{KR_1R_2R_g}{J_2(R_g^2J_1 + J_{p1})s^4 + K(R_2^2R_g^2J_1 + R_2^2J_{p1} + R_1^2J_2)s^2} \quad (11)$$

The single loop plant (Equation 11) relates the output torque to the load position. It was derived using the linear graph in Figure 6.

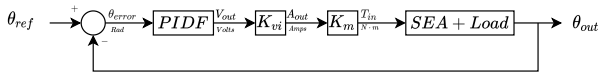

Figure 7: Block diagram of the single loop controller architecture

We attempted to use a PDF (Proportional-Derivative+Filter) for the single loop position controller (Figure 7). The hope was that the lack of an integral term would limit the force output of the device if it was blocked by an obstacle such as human body part. Because there was no integral term, even if there was a persistent position error, the output force would not continue to rise. The plant model (Equation 11) was derived using the linear graph in Figure 6.

Unfortunately, this plant has two poles at the origin and two more poles on the imaginary axis. Because of the placement of these poles, all PDF controllers we designed resulted in closed loop poles in the right half plane, making the system unstable. To reduce this instability, we lowered the aggressiveness of the controller, resulting in some closed loop poles that were barely into the right half plane. Unfortunately, doing so resulted in extremely long predicted rise and settling times and a very low output effort, while still being slightly unstable.

Our model of the plant did not include any damping, and we were hopeful that the small amount of damping present in the actual system would eliminate the predicted instability. Unfortunately, in order to reduce the instability, the PDF controller had a very low gain, and hence a very low output effort, which was not enough to get the system moving at all. Because it was a PDF controller, it had no integral term, so the control effort did not increase despite there being a persistent (steady state) error (difference between the reference position and the actual position).

To fix this problem, we attempted to design a PIDF (Proportional-Integral-Derivative+Filter) con-

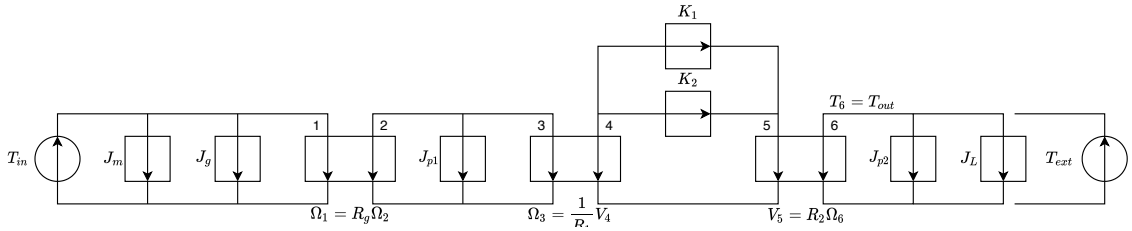

Figure 6: Linear graph of the entire SEA device

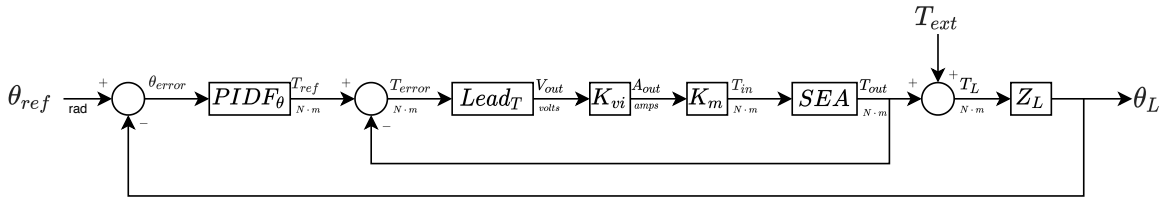

Figure 8: Block diagram of the double loop controller architecture

troller for the single loop, but were unable to design one that was even close to stable and also had a remotely reasonable response time (rise time and settling time). In order to get a working controller for our system, we decided to try a different controller architecture, namely the double loop design.

3.4.2 Double Loop Controller

The double loop controller architecture consists of an outer position control loop around an inner torque control loop, as seen in Figure 8. The outer loop determines the position error and requests the required torque from the inner loop.

$$K_{rot} = K_{lin}R^2 \tag{12}$$

$$T = K_{rot}\theta \tag{13}$$

$$SEA = \frac{T_{out}}{T_{in}} = \frac{KR_1R_2R_g}{(R_g^2(J_1) + J_{p1})s^2 + KR_1^2} \tag{14}$$

The inner loop plant (Equation 14) relates the reference torque to the output torque. To derive this transfer function, we used a simplified linear graph with the load and the disturbance torque removed, as seen in Figure 9.

The inner loop torque controller receives feedback on the output torque by measuring the torque in the springs. The spring torque is calculated by multiplying the spring displacement by the angular spring constant (Equation 13, the rotational spring constant is calculated using Equation 12). The spring displacement is computed based on the angular difference between the powered and the load shafts. The load shaft position is provided by an encoder on the SEA device output shaft, likewise, the powered shaft posi-

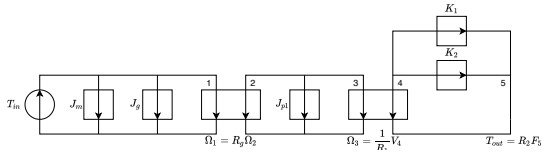

Figure 9: Linear graph of the SEA device with a fixed output (infinite load)

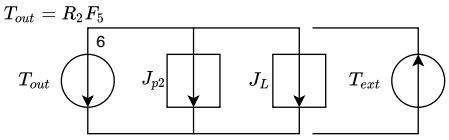

Figure 10: Linear graph of the output load

tion is provided by an encoder on the gearbox output shaft. The inner loop adjusts the output voltage to the motor to track the reference torque provided by the outer loop. The plant model for the inner torque control loop (Equation 14) was derived using the linear graph in Figure 9.

Table 3: Inner Loop Controller Parameters

Zero	$30\,\mathrm{s}^{-1}$
Pole	$228\,\mathrm{s}^{-1}$
Gain	140

MATLAB's `pidtune` function did not seem to be able to design a suitable PIDF controller for the torque controller that had the desired controller effort limits. When we reduced the requested response time in order to reduce the maximum controller effort, `pidtune` was unable to design a controller that produced a stable system. Because of these difficulties with the automated approach, we designed a custom lead controller for the inner torque control loop (MATLAB's `rlocus` function was helpful for visualization of the lead controller design). The chosen parameters can be seen in Table 3.

$$\frac{\Theta_L}{T_{out}} = \frac{1}{J_2 s^2} \tag{15}$$

The load transfer function (Equation 15) relates the output torque to the load position. It was derived using the linear graph in Figure 10.

The outer loop position controller is a PIDF controller that receives feedback on the load position from the encoder on the SEA device output shaft. The outer loop controller computes the torque required to eliminate the error (difference) between the actual position and the reference position, then requests the required torque from the inner loop torque controller. The integral term is necessary to eliminate steady state error in the system. The plant model for the inner torque control loop was derived using the series combination of the inner loop system (the inner loop in Figure 8) and the load transfer function (Equation 15 derived using the linear graph in Figure 10). The chosen controller parameters can be seen in Table 4.

Table 4: Outer Loop Controller Parameters

K_p	$0.0655\,\mathrm{N\,m\,rad}^{-1}$
K_i	$0.0339\,\mathrm{N\,m\,rad}^{-1}\,\mathrm{s}^{-1}$
K_d	$0.0248\,\mathrm{N\,m\,s\,rad}^{-1}$
T_f	$0.0183\,\mathrm{s}$

3.4.3 Controller Design Code

I used MATLAB to design and evaluate the controllers. I modeled the plants as transfer functions using the `tf` function. I used `pidtune` to design the PIDF controllers (and their relatives, PID, PDF, etc.). I used the `rlocus` function to aid in the design of the lead controller. To evaluate the controllers, I

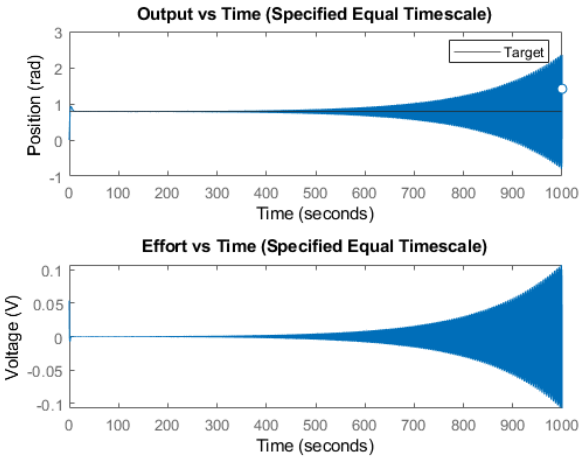

Figure 11: Simulated step response of the single loop position controller

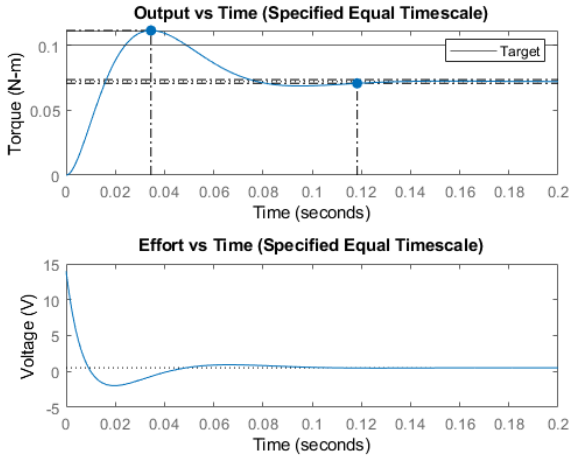

Figure 12: Simulated step response of the inner loop torque controller

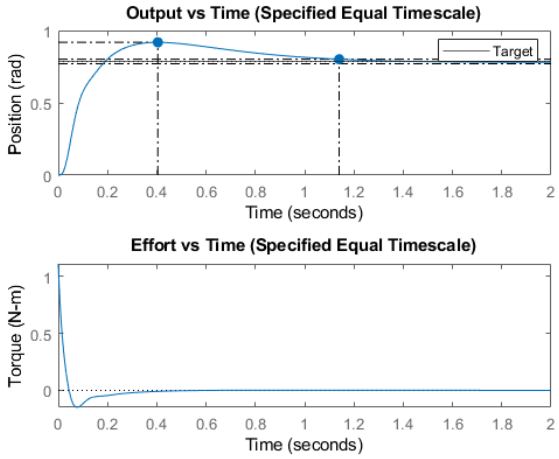

Figure 13: Simulated step response of the double loop position controller

used `step` to check the step response, and `lsim` to simulate the response to a reference signal.

3.4.4 Predicted Performance

Using MATLAB, we simulated the system response to step inputs and to time varying inputs. You can see the simulation results in Figures 11, 12, 13, 14, and 15, and the predicted overall system performance in Table 6.
Comparing the results of our simulation to their target values in Table 5, it is clear we had to make some compromises in the design. The predicted percent overshoot is just above the target value, but the predicted settling time is much greater and the predicted bandwidth is much smaller than their respective target values. The bandwidth miss is possibly due to several commercial models skewing our market average.

The maximum output torque is limited by two factors. One factor is the parameters of the physical system such as the motor torque constant, the amplifier constant, the maximum myRIO output voltage, the maximum amplifier output current, the maximum motor output torque, the maximum current allowed by the motor, the gearbox ratio, and the pulley ratio. The second is the code, as we can limit the myRIO output voltage to anything less than the myRIO's maximum possible output voltage.

Table 5: Functional Requirements vs Simulation Results

Functional Specification	Objective Met
Overshoot	Almost
Settling Time	No
Bandwidth	No
Maximum Output Torque	Set by code

Table 6: Predicted System Performance

Performance Parameter	Value
Rise Time	0.1199 s
Settling Time	1.1399 s
Percent Overshoot	16.8969 %
Bandwidth	$14.45\,\mathrm{rad\,s^{-1}} = 2.3\,\mathrm{Hz}$

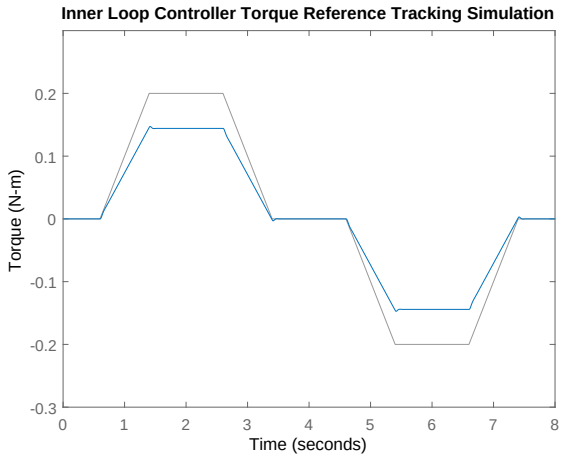

Figure 14: Simulated reference tracking of the inner loop torque controller

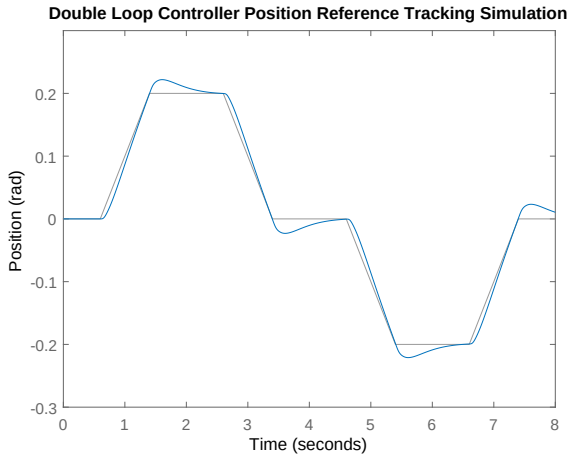

Figure 15: Simulated reference tracking of the double loop position controller

3.5 Electrical

3.5.1 Actuator

The motor used is a Maxon DCX26L 24 volt DC motor. The motor is fitted with a GPX26 planetary gearbox also produced by Maxon which has a gear reduction of 16:1. The motor with attached gearbox produces a maximum torque of 14.4 $N \cdot m$, but due to intentional limiting in the software, the motor will remain well below its maximum value.

3.5.2 Optical Encoders

The encoder measuring the motor side pulley is a compatible quadrature encoder from Maxon that is fit to the rear shaft of the DC motor (figure 4). The encoder measures the rotation of the motor shaft before the gearbox so the gear ratio must be compensated for in software to obtain the pulley rotation. The encoder measuring the load side pulley is a US Digital quadrature encoder attached directly to the output shaft.

3.5.3 Amplifier

The motor is driven by a current amplifier. The myRIO outputs a control voltage which is fed into the amplifier. The amplifier outputs a corresponding current based on its amplification constant of $0.41\,\mathrm{A\,V^{-1}}$. The amplifier is powered from a 110V wall outlet and has a built in emergency stop button to permit manual termination of a test.

3.5.4 Micro-controller

The processor running the control software and interfacing with the electrical components of the system is a Xilinx Zynq-7010 on the National Instruments myRio micro-controller. The myRio has an attached LCD display and keypad that serve as the user interface for the system. A Quanser connector board is attached to the C connector of the myRio and holds the two encoder input channels along with the analog output channel that controls the motor. A simplified wiring schematic is shown in figure 16 and a complete wiring diagram can be found in the appendix.

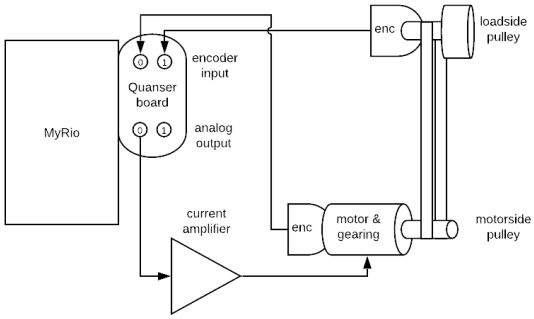

Figure 16: Wiring diagram of our final prototype design

3.6 Embedded Software

3.6.1 C Code on myRIO

The controller is implemented as C code running on a myRIO. The C code is based on Lab 8 from ME 477. It makes use of its main thread to display an interactive table on the LCD display and a separate thread triggered by a timer interrupt to run the controller at a specified sample rate. The main thread runs the `ctable2` command to display an interactive table on the LCD display. The table can be scrolled through using the keypad and displays information about the system in real time, such as the target and actual positions and the output voltage. The interrupt thread is triggered at regular intervals corresponding to the sample rate. When triggered, it performs the steps necessary to control the system.

When running the double loop position controller, the interrupt thread performs the following steps. First, it uses the `sramps` function to compute the reference position. Next, it reads the positions of the two encoders. It computes the position error using the difference between the reference and actual positions. It also computes the actual torque using the difference between the two encoder positions. Next, it computes the reference torque using the `cascade` function, the outer loop controller, and the position error.

Now that the reference torque has been computed, the torque error can be determined by the difference between the reference torque and the actual torque.

This torque error is fed into `cascade` again along with the inner loop controller to compute the output voltage. Finally, this output voltage is sent to the myRIO analog output (AO). If logging is enabled, it also saves all of the relevant values, including the actual and reference positions, the output voltage, the reference torque, and the powered (gearbox output) shaft position to buffers so they can be written to a `.mat` file after the program has terminated.

The `sramps` function accepts a controller as second-order sections representing a discretized transfer function. The controller (as second-order sections), along with other necessary system values, such as the sampling time (T), is included in the project as a C header (`.h`) file. The header file is then included (`#include`) in the `main.c` file that runs on the myRIO after it has been compiled.

3.6.2 MATLAB Interface Code

After the controllers have been designed as continuous time transfer functions in MATLAB, they are discretized using MATLAB's `c2d` function, then converted to second-order sections using `tf2sos`. After that, a script is used to write the second-order sections and other relevant values to the C header file.

After the C program runs on the myRIO, it saves data to a `.mat` file that can be read by MATLAB. After a test run this data can be plotted to determine what the system was doing, what it thought it was doing, and what it was trying to do during its run.

3.6.3 Tools

To write, develop, and run the MATLAB code we used the MATLAB distribution from MathWorks. For C development, we used both Microsoft Visual Studio Code, a lightweight text editor, and Eclipse, an IDE. To track and synchronize our code develop-

ment, we used Git for version control and GitHub for repository hosting.

3.7 Integration

When an external load is applied through the load arm, the spring deforms, and its displacement is calculated based on the angular difference between the powered and the load shafts. The load shaft's position is measured by the load-side encoder while the powered shaft's position is provided by the drive-side encoder. The spring torque is then calculated based on the spring displacement and the spring constant, and is used as the input for the inner loop torque controller. Another input for the inner loop torque controller is the reference torque. The reference torque is computed based on the difference between the reference position and the actual position by the outer loop position controller. The torque error is determined by the difference between the actual and the reference torque. Based on the torque error and using a PIDF controller, the inner loop calculates the required output voltage need to make the motor track the reference torque. This required output voltage is then sent to the myRIO analog output. This process is repeated at regular intervals, thus the motor is able to provide the required torque and adjust the position of the load arm to the reference position.

4 Prototype

4.1 Purpose

The purpose of our prototype is to test the functionality of both the mechanical design and the controller architecture of our SEA device. Simulation of the controller behavior is not sufficient to predict all physical behavior. In particular, damping due to frictional losses are difficult to model accurately for such a complex system and can have a significant effect on controller performance. In order to validate our controller behavior a series of tests needed to be performed. Data was collected on the performance of our prototype for position tracking, position disturbance rejection, and torque tracking. The results of these tests are provided in section 4.3. A photo of the final prototype is provided in Figure 17.

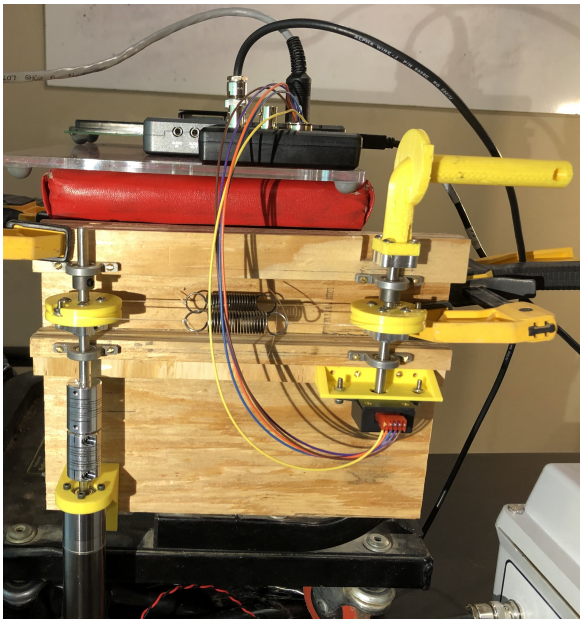

Figure 17: Picture of final prototype

4.2 Description and Implementation

The prototype was based on two 6 mm shafts coupled with various components including couples, hubs, collars, and bearings. The assembly was built on a plywood base made of several layers. While most shaft components were purchased, some fabrication was needed for our pulleys, load arm, motor mount, and load side encoder mount. This fabrication was done using a 3d printer using PLA of 80% infill. Two encoders were used in the prototype in order to achieve inner loop torque control. The drive-side encoder was a Maxon quadrature encoder with 500 CPR. The quadrature encoder on the load-side was one from US Digital with 2000 CPR. Sockets of various weights were used as the loads both for their accessibility and the ease with which they let us change the load inertia. To achieve accurate output arm inertia, the center of mass of these sockets was estimated experi-

mentally through physical balancing. The prototype was controlled using a myRio setup, connected to a test rig with encoder and amplifier communication ports, along with an LCD screen and a keypad. The motor was powered by a 24V amplifier.

4.3 Testing Results

Unfortunately, we were not able to get the single loop position controller to work at all. The output voltage from the PDF controller was not enough to move the load.

4.3.1 Torque Control

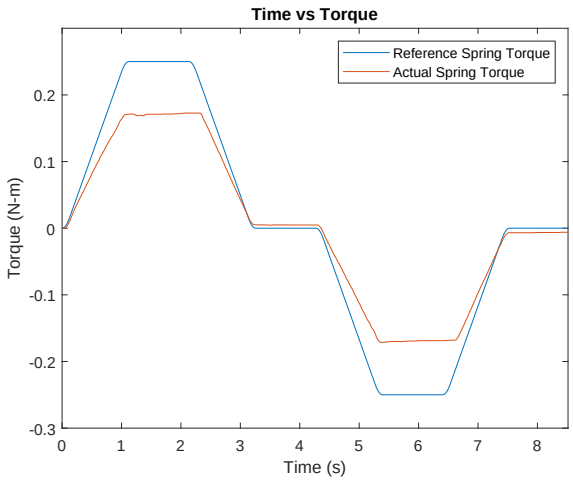

Figure 18: Inner torque control loop reference tracking test results

The inner loop force controller worked much better. To test it, we held the load fixed, and used the `sramps` function to generate a reference torque profile. For testing purposes, a 509 gram mass was fixed to the output load arm. The device was able to track the reference torque quite well, with some steady state error (Figure 18), as predicted by the simulations (Figure 14).

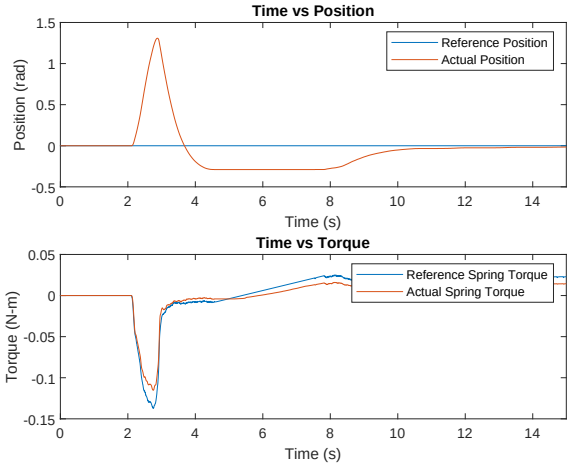

Figure 19: Double position control loop disturbance rejection test results

4.3.2 Position Control

The double loop position controller also worked quite well. To test its reference tracking ability, we used `sramps` to generate a reference position profile. The output position followed the reference position reasonably well (Figure 20). We also tested the disturbance rejection capability of the double loop position controller by setting the reference position to zero and moving the load by hand. When the load was released, it returned to the zero position (Figure 19). It had some overshoot, which was eventually corrected, once the error integral had become large enough that the output voltage was enough to get the load to move.

The prototype overall worked as needed. Some difficulty was had with problems related to miss-ordered parts, but all were overcome with slight modification of the hardware. One issue experienced was a missmatch of shaft size and shaft among the shaft components. It is important to determine which components require a D shaped shaft, which require a circular shaft, which require a press-fit and whether or not you have the capabilities to do so. Other dif-

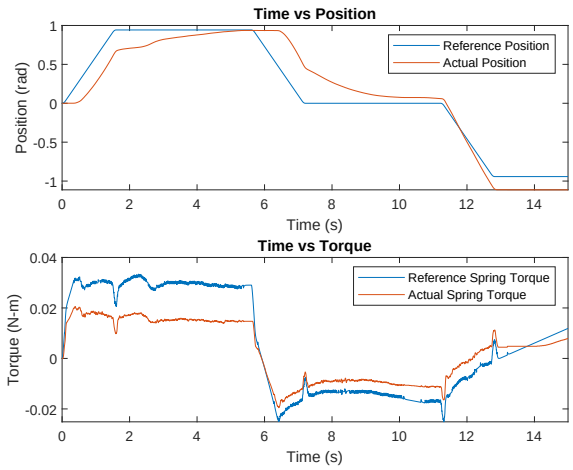

Figure 20: Double position control loop reference tracking test results

ficulties were had related to tensioning the spring, however in the end it was found that a number of coils around the pin while the cable is tied together but non-tensioned is the easiest method.

5 Risk and Liability

There are multiple risks associated with series elastic actuators by virtue of their integral safety-oriented usage in interactive human-robot environments. Because robots have the ability to do damage to humans near them, great care must be taken to ensure that the system always works as intended and fails safely if something does go wrong. Assuming that the system wil not fail in normal operation, another possible risk is a malicious cyberattack that could alter the maximum torque output of the motor and the dynamics of the controller. Advancements in cybersecurity or simply disconnecting the system from the internet have the potential to significantly mitigate this threat.

Moreover, series elastic actuators are widely implemented as anatomical rehabilitation or replacement devices; this advantage is a dangerous risk if a deep medical understanding of human anatomy is not factored into the design. If a design does not consider the medical need for an appropriate response, e.g. bandwidth range and settling time, it could further exacerbate the medical condition. Hence, a holistic approach needs to be followed and an understanding of the human and robotic responses need to be researched and developed thoroughly. Even in instances of perfect compatibility with a subject's motor condition and exoskeletal support need, a controller might need to be versatile and adaptive to the human's neuromuscular needs to enhance recovery [11].

6 Ethical Issues

A major ethical concern for the general public regarding robotic advancement is the replacement of the human workforce. Despite the legitimacy of such fear, in industrial and heavy-manufacturing settings, SEAs augment the safety of human workers and allow them to work more efficiently rather than strictly replace them. Moreover, it is documented that the spread of integrated human-robot workforces in the industry increases overall wealth and that increases the demand sufficiently to counteract the productivity gain [13] .

It is argued that major labor disruptions have occurred in the past that shifted employment needs in a way similar to how human-robot interaction might impact the economy due to SEAs. For instance, 60 percent of the workforce in Europe was employed by farming in the 1800. However, fast-forward past the industrial revolution to the 21st century and only 5 percent of the workforce is involved in farming in the European Union [13]. Furthermore, series elastic actuator applications in the development of exoskeletons have the potential to assist soldiers by providing them with added muscular "power, stamina and weightlifting skills", opening up more ethical dilemmas [1].

Series elastic actuation technology poses the eth-

ical threat of surveillance, increasing government stronghold and limiting personal freedoms. An illustration of such issue is seen in middle of the COVID-19 pandemic where four-legged series-elastic-actuator-driven robots manufactured by Boston Dynamics are deployed in parks in Singapore to encourage social distancing [15], a seemingly positive step but one that that could result in harm with shifting political regimes and philosophies.

7 Impact on Society

Series elastic actuator technology and its ability to reduce output impedance, permit greater shock tolerance and backdrivability, enhanced ability for energy storage and stable force control allowed for the revolutionization of several industrial and healthcare arenas.

In healthcare, SEAs are widely used in gait rehabilitation in knee joint exoskeletons, prostheses and wearable robots, providing medical services that previously required excessive therapy and correctional surgical interventions [7]. SEAs are allowing society to increase its productivity through the integration of the human workforce in heavy-machinery environments, widening the range of manufacturing possibilities that require the proximity of a human and the precision and effectiveness of a robot.

8 Impact on the Environment

The materials used in the manufacturing of series elastic actuators are generally sustainable, as they are widely available metals that are low-cost and easily recyclable. In certain applications of light-weight, less durable, and easily portable SEAs, additive manufacturing could be utilized, which poses a direct environmental impacts due to consumption of plastic feedstocks [6].

SEA systems, especially in assisted therapy, are designed to be extremely compact and portable. This led to the usage of lithium ion technology, which allows for higher power density. The extraction of and manufacturing of the lithium ion battery technology is known to cause water pollution and depletion, and endanger food production and ecosystems due to the toxicity of its chemicals and challenging recyclability [12].

The rapid advancement in energy storage technologies signals a reduction to the negative environmental impacts of SEA technology.

9 Cost and Economics

The major components and their according unit prices are listed in Appendix 12.2. The total cost for purchasing the components and materials is $430.78. The design lasts two quarters, which requires 8 hours work per person per week, and the construction of the prototype takes roughly 30 hours to be finished.

The labor cost is about 830 hours in total, equivalent to an amount of $9960 according to the Washington state minimum wage which is $12 per hour. Thus, the cost for designing and building a single SEA is about $10390.78. Since the design accounts for the most of the total cost, if we consider a mass production of our SEA, as the number of units produced increases, the average cost will drop significantly due to economy of scale.

10 Codes and Standards

The codes and standards used in the design extend from the codes and standards implemented in the manufacturing of the mechanical components; most importantly, the DC motor, the set of encoders and the spring elements.

The Maxon DCX26L motor and the gearbox used to drive the system satisfy the ISO 13485 standards. The ISO 13485 standards manage the quality throughout the life-cycle of a medical device. The implementation of ISO 13485 signals optimal risk

management and high confidence in device performance in medical settings, such as SEA application in assistive therapy and upper and lower limb rehabilitation.

The Maxon DCX26L, the planetary gearhead and the Maxon encoders utilized were produced by Maxon, a company that satisfies the ISO 9001 standard which ensures that the components' manufacturer has "demonstrated their ability to consistently provide products and services that meet customer and applicable statutory and regulatory requirements," [5], which ensures the confidence in the consistency of the components' specifications with the manufacture's provided parameters.

Moreover, although it was not directly used in this project's design, the ANSI/RIA R15.06 safety requirements for industrial robots and robot systems need to be utilized for SEA devices operating in industrial environments. The ANSI R15.06 specifies needed guidelines for a safe design by providing possible hazards and requirements to eliminate them [3].

11 Conclusions

11.1 Continued Development

As discussed in the previous section 4.3.2, the double loop controller design worked quite well, as expected. However, refinements on both the inner and outer loop controller needed to be made for increased control accuracy and stability. The steady state error, as shown in Figure 18, could be further reduced by improving the aggressiveness of the inner loop torque controller, which also allows it to get closer to the reference torque during the double loop operation. Another potential improvement could be made on the current controller design is to increase the integral gain on the outer loop position control in order to improve the settling time for the double loop controller.

For future design iterations we are interested in trying out different control strategies and mechanical designs. One possibility for the controller design is to include a feed-forward term, which could reduce the force control tracking errors where the input torque changes fast. Another idea that is worth trying is the use of variable rate springs instead of conventional springs. For a variable rate spring, its stiffness varies as the externally-applied load changes, thus altering the bandwidth of the controller.

11.2 Final Product Configuration

The final product configuration of our SEA depends on its application. The SEA could be working on its own or several SEAs could be working together. One possible application is for the construction of a robot arm, as discussed in [9], where several SEAs are coupled together to mimic a biological arm. This type of compliant arm could then be used to construct humanoid robots. Another potential application has been demonstrated by the HEBI company, which used a single SEA to build "smart" supporters for equipment, like cameras or other tools, that work safely in a dangerous outdoor environments.

References

[1] From surgeries to keeping company: The place of robots in healthcare. *The Medical Futurist*, October 2019.

[2] Priyanshu Agarwal and Ashish D. Deshpande. Series Elastic Actuators for Small-Scale Robotic Applications. *Journal of Mechanisms and Robotics*, 9(3), 03 2017.

[3] ANSI. Industrial robots and robot systems - safety requirements, 2012. Accessed on 6-12-2020.

[4] Kenan Isik, Shunde He, Joseph Ho, and Luis Sentis. Re-engineering a high performance electrical series elastic actuator for low-cost industrial applications. *Actuators*, 6(1), 2017.

[5] ISO. Quality management systems — requirements, 09 2015. Accessed on 6-12-2020.

[6] Walter; Richter Stephan; Jatzke Tobias; Lessmann Antje; Bovenschulte Marc Keppner, Benno; Kahlenborn. Focus on the future: 3d printing, trend report for assessing the environmental impacts. *Umweltbundesamt*, 5 2018.

[7] Arnaldo Gomes Leal Junior, Rafhael Milanezi de Andrade, and Antonio Bento Filho. Series elastic actuator: Design, analysis and comparison. *Recent Advances in Robotic Systems*, Sep 2016.

[8] Chan Lee, Suhui Kwak, Jihoo Kwak, and Sehoon Oh. Generalization of series elastic actuator configurations and dynamic behavior comparison. *Actuators*, 6(3):26, 2017.

[9] Thomas Lens and Oskar Von Stryk. Design and dynamics model of a lightweight series elastic tendon-driven robot arm. *2013 IEEE International Conference on Robotics and Automation*, 2013.

[10] John Merwin. Fishing Knots: How to Tie the Six Strongest. *Field and Stream*, 08 2019.

[11] David M.Schnyer Michael D. Matthews. Human performance optimization: The science and ethics of enhancing human capabilities. page 505, 2019.

[12] James Murray. Is the nobel prize-winning lithium-ion battery really having a positive impact on the environment?, 10 2019. Accessed on 6-11-2020.

[13] Vincent C. Müller. Ethics of artificial intelligence and robotics. *Stanford Encyclopedia of Philosophy*, 04 2020.

[14] HEBI ROBOTICS. X-series actuator. Accessed on 6-12-2020.

[15] Kevin Stankiewicz. Health and science boston dynamics' dog-like robot spot is being used on coronavirus social distancing patrol, 05 2020. Accessed on 6-11-2020.

12 Appendices

12.1 Final Presentation

Here is a link to the final presentation we gave in ME 495: `https://docs.google.com/presentation/d/177nqU1H-3Xytg2bWvBeavpwNETNy8N8Nge3F7t1YfFI/`.

12.2 Code

The code will be included in the .zip archive with this report. It is also available online at `https://github.com/SometimesCalledJim/Mechatronics-Capstone`.

12.3 Drawings

12.3.1 Electrical

Figure 21: MyRio Device

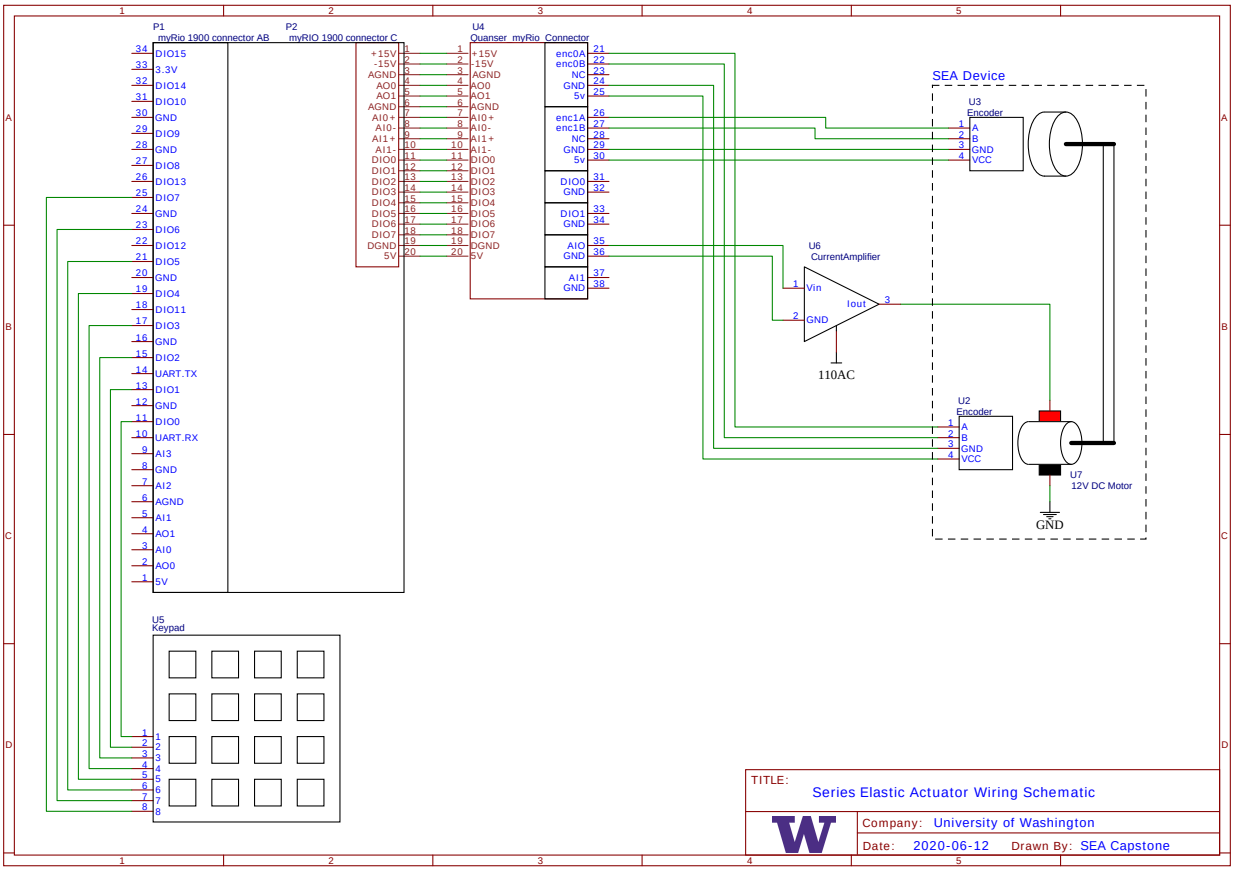

Figure 22: Wiring Schematic

12.4 Major Components of Prototype

Description	Manufacturer	Model Number	Unit price ($)	Quantity
Encoder(drive-side)	Maxon	110517	0	1
Planetary gearbox	Maxon	GPX 26	0	1
Motor	Maxon	DCX26L	0	1
Current amplifier	N/A	N/A	0	1
myRio amplifier cable	N/A	N/A	0	1
myRio signal input module and connector	N/A	N/A	0	1
Amplifier to motor cable	N/A	N/A	0	1
Shaft coupler	McMaster-Carr	2464K15	48.44	2
Shaft	McMaster-Carr	1265K53	32.69	1
Shaft collar	McMaster-Carr	6056N14	1.74	2
Bearing	McMaster-Carr	8600N12	31.68	4
Extension Spring (3.3lbf/in) (3 units)	McMaster-Carr	9044K319	5.6	1
Extension Spring (7.7lbf/in) (3 units)	McMaster-Carr	9044K112	8.14	1
Extension Spring (16.4lbf/in) (3 units)	McMaster-Carr	9044K145	5.26	1
Extension Spring (38.6lbf/in) (3 units)	McMaster-Carr	9044K114	8.14	1
Extension Spring (57.6lbf/in) (3 units)	McMaster-Carr	9044K139	5.26	1
Shaft hub	Servo City	545578	5.99	3
Encoder (load-side)	US Digital	E2-2000-236-IE-D-G-3	76.53	1
Encoder cable	US Digital	CA-C5-W5-NC-1	5.75	1
#5 1/8” wood screw (100 count)	McMaster-Carr	92407A081	5.36	1
6-32 hex bolt (100 count)	McMaster-Carr	92949A148	3.72	1
#5 bolt (50 count)	McMaster-Carr	92196A128	3.14	1
#5 Nut (100 count)	McMaster-Carr	90730A006	5.66	1
#5 Washer (100 count)	McMaster-Carr	92141A006	1.43	1
Nylon Fishing Cable (300 yrds)	Lonpar	N/A	15.99	1
1/2 inch plywood 12”x12”	McMaster-Carr	1125T516	1.53	2
Total cost ($)	430.78			